Transverse field muon-spin rotation signature of the skyrmion-lattice phase in Cu$_2$OSeO$_3$

T. Lancaster,[1,*] R. C. Williams,[1] I. O. Thomas,[1] F. Xiao,[1] F. L. Pratt,[2] S. J. Blundell,[3] J. C. Loudon,[4] T. Hesjedal,[3] S. J. Clark,[1]
P. D. Hatton,[1] M. Ciomaga Hatnean,[5] D. S. Keeble,[5] and G. Balakrishnan[5]

[1]*Centre for Materials Physics, Durham University, Durham, DH1 3LE, United Kingdom*
[2]*ISIS Facility, STFC Rutherford Appleton Laboratory, Chilton, Didcot, Oxfordshire, OX11 0QX, United Kingdom*
[3]*Oxford University Department of Physics, Clarendon Laboratory, Parks Road, Oxford, OX1 3PU, United Kingdom*
[4]*Department of Materials Science and Metallurgy, University of Cambridge, 27 Charles Babbage Road,*
Cambridge CB3 0FS, United Kingdom
[5]*University of Warwick, Department of Physics, Coventry, CV4 7AL, United Kingdom*

We present the results of transverse field (TF) muon-spin rotation (μ^+SR) measurements on Cu$_2$OSeO$_3$, which has a skyrmion-lattice (SL) phase. We measure the response of the TF μ^+SR signal in that phase along with the surrounding ones, and suggest how the phases might be distinguished using the results of these measurements. Dipole field simulations support the conclusion that the muon is sensitive to the SL via the TF line shape and, based on this interpretation, our measurements suggest that the SL is quasistatic on a time scale $\tau > 100$ ns.

I. INTRODUCTION

The understanding of matter and its excitations in terms of topology has a long history which is now allowing us an insight into the properties of quantum materials and the opportunity for their manipulation. Topological physics includes the study of kinks, vortices, and monopoles in quantum field theory, which forms the basis of a successful branch of condensed matter physics [1,2]. A skyrmion [3] is a topological object which has been shown to exist in a range of magnetic materials at particularly well-defined conditions of temperature and magnetic field. The simplest example of a skyrmion may be derived from a sphere studded with arrows pointing radially. A skyrmion is formed if we stereographically project the arrows onto a plane while keeping their orientations fixed. This produces a twisting pattern which turns out to be a stable knot; it cannot be untied as long as the fields remain smooth and finite. While skyrmions exist in different forms in a variety of physical systems, the clearest evidence for the existence of the skyrmion is in the spin texture of magnetic systems, and in recent years a number of spectacular advances have demonstrated not only the existence of magnetic skyrmions, but also their ordering into a skyrmion lattice (SL) [4–13]. There is considerable similarity between the SL, which has recently been shown to be present in a range of noncentrosymmetric, helimagnetic systems, and another topological phase: the vortex lattice (VL) found in type-II superconductors in applied magnetic field. Like the SL, the superconducting VL leads to a textured, periodic distribution of magnetic field within the body of the material, which is large on the scale of the crystallographic unit cell. In practice, the same experimental techniques that have been successfully applied to probing VL physics, such as small-angle neutron scattering [14] and, in particular, muon-spin rotation (μ^+SR) [15,16], could potentially be applied to probe the physics of the SL and this hypothesis forms the basis of the work reported here. In this paper, we investigate the extent to which transverse

field (TF) μ^+SR measurements are sensitive to the skyrmion phase in the multiferroic skyrmion material Cu$_2$OSeO$_3$.

Our use of TF μ^+SR to probe the SL in Cu$_2$OSeO$_3$ is analogous to its use in probing the VL in a type-II superconductor, where the technique provides a powerful means of measuring the internal magnetic field distribution caused by the presence of the magnetic field texture [15,16]. In a TF μ^+SR experiment, spin-polarized muons are implanted in the bulk of a material, in the presence of a magnetic field $B_{\rm a}$, which is applied perpendicular to the initial muon-spin direction. Muons stop at random positions on the length scale of the field texture where they precess about the total local magnetic field B at the muon site (mainly due to the field texture), with frequency $\omega = \gamma_\mu B$, where $\gamma_\mu = 2\pi \times 135.5$ MHz T^{-1}. The observed property of the experiment is the time evolution of the muon-spin polarization $P_x(t)$, which allows the determination of the distribution $p(B)$ of local magnetic fields across the sample volume via $P_x(t) = \int_0^\infty dB\, p(B) \cos(\gamma_\mu B t + \phi)$ where the phase ϕ results from the detector geometry.

For our measurements, powder and single-crystal samples of Cu$_2$OSeO$_3$ were synthesized as described previously [17], with the same batch of polycrystalline powder also used for the growth of single crystals using the chemical vapor transport technique. The samples were characterized with powder and single-crystal x-ray diffraction which confirmed that the samples were of the requisite B20 phase. The magnetic response was checked with magnetic susceptibility measurements which confirmed the magnetic transition observed at $T = 57$ K.

To establish the existence of skyrmions in our Cu$_2$OSeO$_3$ samples, a sample was prepared for electron microscopy. Single-crystal samples showed clear facets and the sample was mechanically polished on a (110) face until it was 20 μm thick. It was then further thinned by argon ion beam irradiation using a Gatan Precision Ion Polishing System (PIPS) initially operated at 4 kV with the ion guns set at 7° to the sample plane. Once the sample thickness approached the wavelength of light, rainbow colors could be observed using an optical microscope and, at this point, the voltage was reduced to 2 kV and the gun angle to 5° and thinning continued until

————————
*tom.lancaster@durham.ac.uk

a hole of size 15 μm appeared. Images were taken from an area of sample approximately 50 nm thick surrounding this hole with an FEI Tecnai F20 transmission electron microscope (TEM) equipped with a field-emission gun using an acceleration voltage of 200 kV. In normal operation, the objective lens of the microscope applies a 2 T field to the specimen which would force it into its ferrimagnetic state so images were acquired in low-magnification mode in which the image is formed using the diffraction lens and the objective lens was weakly excited to apply a small magnetic field normal to the plane of the specimen. The sample was cooled using a Gatan liquid-helium-cooled IKHCHDT3010-special tilt-rotate holder which has a base temperature of 10 K. The images were recorded on a CCD using a Gatan Imaging Filter and they were energy filtered so that only electrons which had lost between 0 and 1 eV on passing through the specimen contributed to the image. An aperture was also used to ensure that only the 000-beam and the low-angle scattering from the skyrmions contributed to the image. The defocus and magnification were calibrated by acquiring images with the same lens settings from Agar Scientifics S106 calibration specimen, which consists of lines spaced by 463 nm ruled on an amorphous film. The defocus was found by taking digital Fourier transforms of the images acquired from the calibration specimen and measuring the radii of the dark rings that result from the contrast transfer function as previously described [18]. These TEM measurements on the thinned crystallites confirm the presence of skyrmion spin textures, as shown in Fig. 1. These occur over an extended region of the phase diagram, compared to results on bulk materials, as observed previously [8]. We also note the coexistence of skyrmions and helices, as seen in the previous microscopy study [8].

TF μ^+SR measurements were made using the MuSR spectrometer at the ISIS facility and the GPS spectrometer at the Swiss Muon Source (SμS). For measurements at ISIS, the sample was mounted on a hematite backing plate in order that muons that are implanted in the hematite would be rapidly depolarized and therefore removed from the spectrum. For measurements at GPS, the so-called flypast geometry was employed, where the powder sample was suspended on a fork, which prevents those muons that do not implant in the sample from contributing to the signal. For all measurements presented, the sample was cooled from $T > 60$ K in the applied field. All data analysis was carried out using the WIMDA program [19].

II. RESULTS OF TF μ^+SR MEASUREMENTS

The region of the Cu$_2$OSeO$_3$ phase diagram of interest in this study is shown in Fig. 2(a). We note that this is the phase diagram from Ref. [8], which differs slightly from that derived from other studies (e.g., Refs. [12,13]). In this material, spins are located on the Cu^{2+} ions, which are arranged in four tetrahedra within the unit cell. Ferrimagnetic (FiM) ordering of these spins is favored, with one Cu ion (Cu1) oriented in the opposite direction to that of the others (Cu2) [17,20]. This ordered configuration persists when we build more complicated spin configurations described in the following [21]. In systems such as Cu$_2$OSeO$_3$ which lack
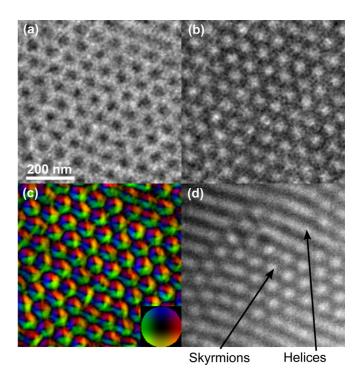

FIG. 1. (Color online) (a), (b) Skyrmions in Cu$_2$OSeO$_3$ imaged with Lorentz TEM at 10 K in a field of 30 mT with defoci ±0.7 mm. (c) Magnetic induction map constructed from (a) and (b) using the transport of intensity equation. The direction of the local induction is indicated by the color wheel (inset). (d) Skyrmions coexisting with the helical phase at 30 K in a field of 40 mT. Similar observations were made by Seki *et al.* [8].

inversion symmetry, chiral interactions are capable of stabilizing helically ordered configurations of spins [22]. An applied external magnetic field can further stabilize a superposition of three helical configurations in the plane perpendicular to the field (the configuration is translationally invariant in the remaining direction). Skyrmion spin textures can be formed from a triangular arrangement of the wave vectors of these helices [23]. From the Cu$_2$OSeO$_3$ phase diagram, we see that below a lower critical field a phase described as the multi-q helimagnetic (or simply the helimagnetic phase) exists. In bulk single-crystal samples, this consists of multiple domains of helimagnetic stripes whose q vectors are aligned along the three $\langle 001 \rangle$ directions [9,12]. Above this lower critical field but below a second, larger critical field (above which there is a transition to a ferrimagnetic phase), the q vector is aligned parallel to the direction of the field, forming a single-q helimagnetic phase (also called the conical phase) where there are no multiple domains [8,9,12]. In Cu$_2$OSeO$_3$, the A phase or skyrmion-lattice phase (often denoted SkX) is centered around $B_a = 30$ mT at $T = 57$ K, close to the critical temperature T_c where the system undergoes a transition to a paramagnetic state [8,9,12]. The SkX phase may be described by a phase-locked superposition of three helimagnetic textures with q vectors perpendicular to the direction of the field, such that a regular lattice of skyrmions is formed. It has further been shown in a bulk single-crystal system that this phase may be further subdivided into two subphases, with the lattice in the second being rotated by 30° with respect to the lattice in the
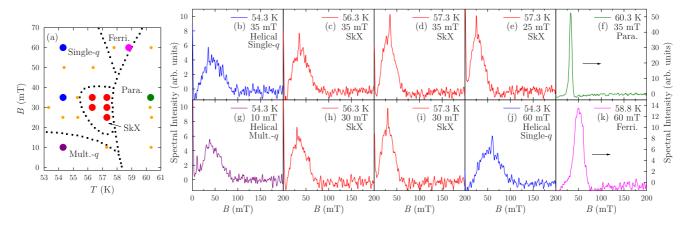
FIG. 2. (Color online) (a) The phase diagram of Cu_2OSeO_3, indicating the locations of the paramagnetic, ferrimagnetic, single-q, and multiple-q helical phases. Small circles show where measurements were taken, and the bold circles correspond to the frequency spectra displayed in (b)–(k). These phase boundaries are taken from Ref. [8]. (b)–(k) Evolution of the magnetic field distribution measured at SμS, with temperature and applied field. (b), (j) Single-q helical phase; (c)–(e), (h), (i) the SkX phase containing the SL; (f) paramagnetic phase; (g) the multi-q helical phase; and (k) the ferrimagnetic phase. All data are plotted to the same spectral intensity scale, except (f) and (k).

first [9]. The range of applied magnetic fields over which the SkX phase occurs in Cu_2OSeO_3 makes it well matched to the ISIS and the SμS muon source time windows.

Example TF μ^+SR time-domain spectra measured at SμS are shown in Fig. 3, where the increase in damping upon entering a magnetically ordered phases (in this case, the skyrmion and single-q phases) is evident. For our purposes, it is more instructive to consider the frequency domain spectra, as shown in Figs. 2 and 4. These were obtained via a fast Fourier transform of the time-domain spectra, using a Lorentzian filter with time constant 2.2 μs. [In these spectra, the spectral density is proportional to $p(B)$.]

We see that spectra in the skyrmion phase are characterized via a relatively narrow, asymmetric spectral density distribution, which rises steeply on the low-field side leading to a sharp peak, when compared to spectra within the helical phases. This peak then decays, first very rapidly and then more gradually with increasing field. In contrast, the single-q and multi-q helical phases give rise to less asymmetric distributions with broader maxima and spectral weight distributed over a larger range of fields. In further contrast, the ferrimagnetic phase shows a narrowed, fairly symmetric line, while the
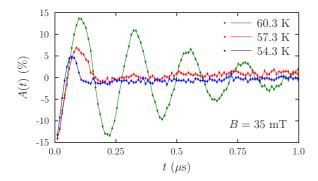
paramagnetic regime is characterized by a very narrow linewidth (note the change of scale in Fig. 2 for spectra from these latter two phases).

Spectra in the single-q phase do not show a significant change with temperature below 55 K. However, as we approach temperatures close to the transition to the paramagnetic region (Fig. 4), we see a temperature-driven effect in the single-q, multi-q, and skymion regions, which causes the spectra to show more spectral weight at the applied field, taking on a more heavily peaked appearance. This effect is evident in several spectra [see, e.g., Fig. 4(d)], but can be most clearly seen in the single-q phase data measured at 50 mT and 56.3 K [Fig. 4(b)] when compared to spectra measured

FIG. 3. (Color online) (a) Time-domain spectra measured in an applied transverse magnetic field of 35 mT in the paramagnetic phase at 60.3 K, the skyrmion phase at 57.3 K, and the single-q phase at 54.3 K.
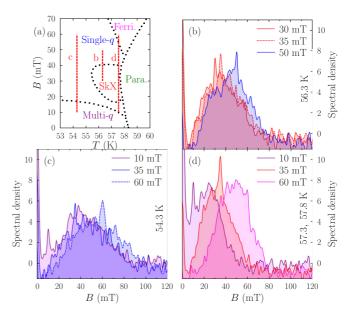

FIG. 4. (Color online) (a) The cuts through the phase diagram at constant temperature displayed in (b)–(d). (b) Applied magnetic field dependence of the TF line shape measured at $T = 56.3$ K. (c) Field sweep within the multi-q and single-q phases at 54.3 K. (d) Field sweep through multi-q, SkX, and ferrimagnetic phases.
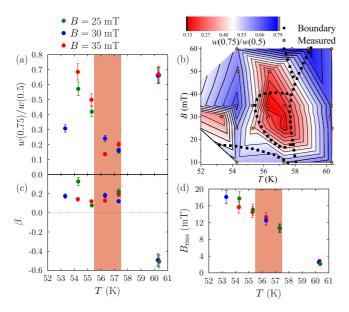
FIG. 5. (Color online) (a) The ratio of peak widths $w(0.75)/w(0.5)$ discussed in the text. (b) Contour plot of $w(0.75)/w(0.5)$ from which the SkX phase may be identified. (c) The skewness β and (d) standard deviation B_{rms} as a function of temperature.

at lower temperature in that phase [Fig. 4(c)], which are quite unresponsive to changes in applied field. However, comparing this latter single-q phase spectrum with those measured at the same temperature, but in fields thought to promote the SkX phase [Fig. 4(b)], we see that the spectra may still be distinguished: the SkX-phase spectra are more asymmetric, with spectral weight persisting on the high-field side of the peak. We note that in the Lorentz TEM measurements there is evidence for the coexistence of skyrmions and helical spin textures [Fig. 1(d)]. It could be, therefore, the case that the data point in question ($B = 50$ mT and $T = 56.3$ K), measured on a polycrystalline sample, features a contribution from both single-q and SkX phases. However, it is also worth recalling that the phase diagram of the thinned samples supports the existence of skyrmions over a wider range of the B-T phase diagram than for the bulk, so the cases are not straightforwardly comparable.

One crude way to identify the SkX region of the phase diagram from these data is via the relatively tapered line shape observed in that phase. To this end, Fig. 5(a) shows one possible parametrization of our data that approximately captures the characteristic signal in the SkX region. In Fig. 5(a), we show the ratio of $w(0.75)$ (the full peak width at 0.75 of the maximum spectral weight) to $w(0.5)$ (the full width at half maximum). The contour plot in Fig. 5(b) shows that this quantity picks out the SkX phase as an island centered around 57 K and 30 mT where $w(0.75)/w(0.5)$ is suppressed. Moreover, despite the resolution of our contour plot being limited by the number of data points, we note the resemblance to the skyrmion phase boundaries reported elsewhere. Most of the spectra obtained outside of the paramagnetic region display a small additional peak at the value of the applied field, which we ascribe to the diamagnetic response from a small portion of the muon ensemble. This might cause a further suppression of $w(0.75)/w(0.5)$ within the SkX phase, whose suppression is otherwise caused

by the tapered nature of the line shape, as the diamagnetic contribution coincides with the peak in spectral weight in the muon response caused by the internal field distribution. The limitation of this method is apparent, however, in that the data point at 50 mT and 56.3 K discussed above gives a rather similar ratio to the points in the SkX region, despite its line shape being distinguishable via its asymmetry. As described above, one interpretation of this spectrum involves some portion of the signal arising from skyrmions, but it remains distinct from the other spectra from the SkX phase, suggesting that there is a significant single-q phase contribution.

The normalized skewness of the distribution β, defined via $\beta = \int dB \, p(B) [\frac{(B - \langle B \rangle)}{B_{\mathrm{rms}}}]^3$, is shown in Fig. 5(c). We find that β is slightly enhanced in the SkX phase compared to the single-q phase, before dropping to a negative value in the paramagnetic (PM) phase. Finally, the standard deviation Fig. 5(d) of the distribution $B_{\mathrm{rms}} = \sqrt{\langle (B - \langle B \rangle)^2 \rangle}$ increases fairly smoothly with decreasing temperature, but is less sensitive to the SkX phase boundaries.

Our results suggest that TF μ^+SR is sensitive to the SkX phase through the muon line shape. Assuming that this is the case, we may consider the mechanisms for muon relaxation and the time scales involved. We note that, in contrast to muon spectroscopy, neutron measurements of the SL are insensitive to fluctuations on time scales much slower than $\hbar/\Delta E \approx 10^{-11}$ s (where $\Delta E \approx 1$ meV is the energy scale of the resolution of the measurement) and so fluctuations on time scales longer than this appear static. Neutrons therefore take a "snapshot" of the behavior compared to μ^+SR measurements whose characteristic time scale is set by the gyromagnetic ratio of the muon ($\gamma_\mu = 2\pi \times 135.5$ MHz T^{-1}). The sensitivity of the muon to the SL would imply that the signal from the long-range spin texture is not significantly motionally narrowed. This would imply that the SL itself is likely to be quasistatic on time scales $\tau \gg (1/\gamma_\mu B_{\mathrm{rms}}) > 100$ ns. This is consistent with the long lengthscale dynamics observed via Lorentz microscopy [24], which suggest rotations of the skyrmion texture take place on a 0.1 s timescale. Consistent with the observation that the muon signal below T_c is dominated by the the distribution of static internal magnetic fields are the results of the previous zero-field μ^+SR study of this material [20]. Those measurements showed sizable transverse relaxation of the muon precession signal, which decreased as the transition was approached from below, consistent with the decrease of the internal field with increasing temperature. This was accompanied by an increase in a small longitudinal relaxation rate, suggesting a slowing of residual dynamic fluctuations above 50 K (i.e., in the region of interest for our study). It might be expected that the nature of the dynamics changes in each of the magnetic phases. However, the contribution to the muon linewidth from the dynamic effects would seem to make only a small contribution to the overall shape.

Further TF measurements were also made on a powder sample at ISIS using the MuSR instrument. In this case, we obtain similar responses as those reported above, although the analysis of these are complicated by a sizable background contribution from muons stopping in the sample holder or cryostat tails. Example frequency spectra, obtained via maximum entropy analysis of the measured time-domain spectra, are shown in Fig. 6 for cuts through the SkX phase
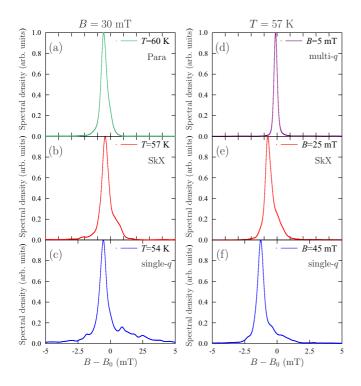
FIG. 6. (Color online) Evolution of the magnetic field distribution (measured at ISIS) for measurements made on a powder sample in a field of 30 mT (a)–(c) and at a temperature of 57 K (d)–(f). (a) Paramagnetic phase; (b), (e) the SkX phase containing the SL; (c), (f) single-q helical phase; and (d) multi-q phase.

in field and temperature. In these we see that a knee in the spectrum develops in the SkX phase [Figs. 6(b) and 6(e)] on the high-field side of the peak region [Fig. 6(a)]. This corresponds to the slow decay of the line shape in high field seen in the SμS data in Fig. 2. This feature is lost when we enter the single-q phase [Figs. 6(c) and 6(f)], where the spectral weight in the knee is seen to decay into a broad distribution. In the multi-q phase, the line is seen to be very narrow, suggesting that the background contribution is dominant in this case.

Measurements were repeated on other batches of powder sample, which showed some slight deviations in the position of the phase boundary to the paramagnetic phase, which we attribute to sample variability. We also made measurements at ISIS on mosaics of unoriented single-crystal samples, which showed consistent results, although the lack of angular averaging and some sample variability makes a detailed comparison difficult.

III. DISCUSSION

In order to understand these results, we have simulated the expected distribution $p(B)$ for the spin configurations of this material. Owing to the complexity of the problem in a system with multiple muon sites and a complicated spin configuration, we have simulated the field distributions expected for a single-crystal orientation, with the applied magnetic field along [001]. For simplicity, we generate our skyrmion spin textures here using the three-q approach outlined in the following. We note that more sophisticated treatments of the SL are

possible (e.g., Ref. [25]), whose predictions are generally in better agreement with observations. For our simulation, skyrmionlike spin configurations [4,10] were generated using $\boldsymbol{m}(\boldsymbol{r}) = \boldsymbol{m}_{\rm sk}(\boldsymbol{r})/|\boldsymbol{m}_{\rm sk}(\boldsymbol{r})|$ where

$$\boldsymbol{m}_{\rm sk}(\boldsymbol{r}) = \sum_{i=1}^{3} [\hat{\boldsymbol{e}}_z \cos(\boldsymbol{q}_i \cdot \boldsymbol{r} + \pi) + \hat{\boldsymbol{e}}_i \sin(\boldsymbol{q}_i \cdot \boldsymbol{r} + \pi)], \quad (1)$$

where $\boldsymbol{q}_i$ are the skyrmion-lattice modulation vectors, taken to be perpendicular to the applied field $B_{\rm a}$ ($\parallel \hat{\boldsymbol{e}}_z$), and $\hat{\boldsymbol{e}}_i$ are the unit vectors of the skyrmion lattice (also perpendicular to $B_{\rm a}$). We generate a skyrmion-lattice magnetization texture in the [110] plane by taking $\boldsymbol{q}_1 = F(-1, 0, 0)$, $\boldsymbol{q}_2 = F(\frac{1}{2}, -\frac{\sqrt{3}}{2}, 0)$, $\boldsymbol{q}_3 = F(\frac{1}{2}, \frac{\sqrt{3}}{2}, 0)$, $\hat{\boldsymbol{e}}_1 = (0, 1, 0)$, $\hat{\boldsymbol{e}}_2 = (-\frac{\sqrt{3}}{2}, -\frac{1}{2}, 0)$, and $\hat{\boldsymbol{e}}_3 = (\frac{\sqrt{3}}{2}, -\frac{1}{2}, 0)$, where $F = 2\pi/L_{\rm sk}$ and $L_{\rm sk}$ is the skyrmion wavelength. For our simulations, we used a value of $L_{\rm sk} = 70$ unit cells, similar to that suggested in Ref. [9]. This method results in a ferromagnetic (FM) ordering of the spins within a crystalline unit cell. By reversing the spin on the Cu1 sites, we generate ferrimagnetic (FiM) configurations, which result in textures that match the observed magnetic structures of the system [17].

In addition to the SL, we have generated spin textures for the helical phases. Single-q helical configurations were calculated for $B_{\rm a}$ parallel to the [001] direction using [10]

$$\boldsymbol{m}(\boldsymbol{r}) = -\frac{1}{2} [\hat{\boldsymbol{e}}_x \cos(q_z z) + \hat{\boldsymbol{e}}_y \sin(q_z z)], \quad (2)$$

where $q_z = 2\pi/L_{sk}$. Reversing the Cu1 spin direction again generates the FiM configurations. The exact spin configuration of the more complicated multi-q phase is not confirmed and so we have investigated a trial structure. We chose to model this phase by calculating the field distributions for FiM configurations reflecting six possible domains, each with equal population. Each domain has $\boldsymbol{q}$ either parallel or antiparallel to the [100], [010], or [001] axes. Its texture is given by $\boldsymbol{m}(\boldsymbol{r}) = \frac{1}{2} [\hat{\boldsymbol{e}}_i \cos(\boldsymbol{q} \cdot \boldsymbol{r}) + \hat{\boldsymbol{e}}_j \sin(\boldsymbol{q} \cdot \boldsymbol{r})]$ where $\hat{\boldsymbol{e}}_i$ and $\hat{\boldsymbol{e}}_j$ are unit vectors in the plane perpendicular to $\boldsymbol{q}$ and $\boldsymbol{q} = \pm \hat{\boldsymbol{e}}_q |\boldsymbol{q}|$ for the parallel and antiparallel cases, respectively. Here, $\hat{\boldsymbol{e}}_q$ is the unit vector in the direction of $\boldsymbol{q}$ and $|\boldsymbol{q}| = 2\pi/L_{\rm sk}$. We average over the distributions for the six resulting textures in order to obtain our overall distribution.

We assume muons couple to the dipolar magnetic fields of the Cu^{2+} spins in the material. The dipole magnetic field component B^i at a position $\boldsymbol{r}$ is given by [15,20]

$$B^i(\boldsymbol{r}) = \frac{C\mu_0}{4\pi} \sum_{n,j} \frac{m^j(\boldsymbol{r}_n)}{R_n^3} \left(\frac{3R_n^i R_n^j}{R_n^2} - \delta^{ij} \right) + B_{\rm a}, \quad (3)$$

where i and j run over all three Cartesian directions, n labels a Cu ion at position $\boldsymbol{r}_n$, $C = 0.25/\sqrt{3}$ scales the magnetic moment to match that observed for Cu ions in these systems (see below) and $\boldsymbol{R}_n = \boldsymbol{r} - \boldsymbol{r}_n$. A previous zero-field μ^+SR study of this material [20] found five muon stopping sites in each crystalline unit cell at positions $A = (0.215, 0.700, 0.970)$, $B = (0.035, 0.720, 0.805)$, $C = (0.195, 0.555, 0.795)$, $D = (0.275, 0.295, 0.460)$, and $E = (0.635, 0.550, 0.525)$. We have simulated the field distribution $p(B)$ expected in each of the phases at a variety of applied magnetic fields, assuming these previously proposed muon sites. For these simulations,
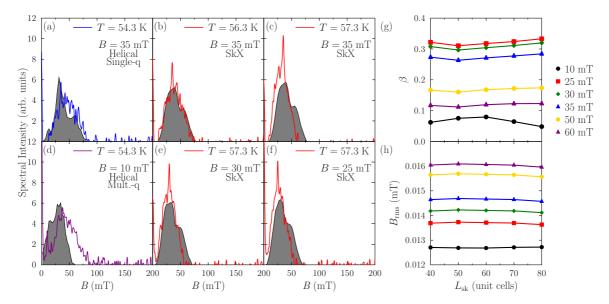
FIG. 7. (Color online) (a)–(f) Results of dipole simulations of $p(B)$ in each phase (shown shaded) compared with the spectra measured at SμS. In order to compare the simulation and experiment, the area under the simulated distribution is scaled to that under the experimental distribution, assuming a constant background contribution. Scaling of the (g) skewness and (h) B_{rms} of the simulated distribution with the skyrmion lattice size L_{sk}.

we take the magnetic moment to be $0.25\mu_B$, consistent with that found in a previous study [17]. For comparison with the measured spectra, the distributions were convolved with a simulated instrument function, generated with the WIMDA program.

The results of these simulations are compared with the observed spectra in Fig. 7. We see that the simulations capture the line shape in the skyrmion regime quite well and are distinguishable from the predicted line shapes in the other magnetic phases. Although the agreement for the single-q helical phase is reasonable, a discrepancy is evident in the multi-q helical phase, as might be expected if the trial structure is not the correct one. (It is possible in this case that an alternative trial structure would produce results that match the measured spectra more closely.) We note that our results appear to be consistent with magnetic moments being localized on the Cu^{2+} ions, as was found from x-ray measurements [11] (although it is possible that a delocalized arrangement would match the data more closely in the multi-q phase).

The simulations may also be used to test whether the muon line shape has a sensitivity to the lengthscale L_{sk} that characterizes the SL. Plots of the width B_{rms} and skewness β against L_{sk} are shown in Fig. 7, where we see that there is little variation with L_{sk}. It would therefore be difficult for this system to determine the L_{sk} in the absence of other detailed information about the phase, such as the magnetic structure, muon sites, and moment sizes.

To gain some insight into how the field distributions shown in Fig. 7 arise from the SkX phase spin textures, we may consider the dipole fields produced by a skyrmion at individual muon sites. In Cu_2OSeO_3, this is complicated by the large number of inequivalent muon sites [20] and the ferrimagnetic arrangements of Cu^{2+} spins that form the basis of the skyrmion spin texture. Figures 8(a) and 8(b) show examples of the magnitude of the dipole field found at two of the five crystallographically distinct muon sites, evaluated

across a single skyrmion. The corresponding field distribution $p(B)$ derived from each is also shown [Figs. 8(c) and 8(d)]. The skyrmion texture is shown to give rise to an asymmetric
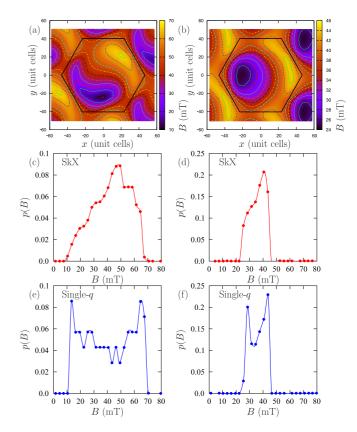

FIG. 8. (Color online) The magnitude of the dipole field at the (a) A and (b) E muon sites due to a skyrmion in an applied field of $B_a = 35$ mT. Field distribution for SkX phase at (c) A and (d) E sites. Field distribution for the single-q phase at (e) A and (f) E sites.

field distribution at each site, with spectral weight skewed towards high fields. When summed over all muon sites, these individual distributions produce the total $p(B)$ distribution shown in Fig. 7. These distributions may be contrasted with those found in the single-q helical phase [Figs. 8(e) and 8(f)], which are more symmetrical. It is difficult from these results to make general predictions regarding the dipole field distribution expected from other skyrmion materials, beyond the expectation of asymmetric field distributions at each muon site. We note that this complexity for the SL spectrum is in marked contrast to the relative simplicity of the VL spectrum, where characteristic spectral features map directly onto special positions within the VL.

In conclusion, we have presented results that suggest that TF μ^+SR is sensitive to the skyrmion lattice via measurements similar to those carried out on the vortex lattice in type-II superconductors. This would imply that in Cu_2OSeO_3 the SL is static on a time scale $\tau > 100$ ns. We are also aware of independent work currently being prepared for publication [26] that demonstrates that longitudinal field μ^+SR measurements [27] are also sensitive to the skyrmion phase via changes in the spin dynamics. Taken together, these results suggest that in favorable cases μ^+SR could be utilized as a method for identifying skyrmionic materials, characterizing the behavior of the skyrmion lattice and deriving their phase diagrams.

[1] P. M. Chaikin and T. C. Lubensky, *Principles of Condensed Matter Physics* (Cambridge University Press, Cambridge, UK, 1990).

[2] N. Nagaosa and Y. Tokura, Nat. Nanotechnol. **8**, 899 (2013).

[3] T. H. R. Skyrme, Proc. R. Soc. London, Ser. A **260**, 127 (1961); Nucl. Phys. **31**, 556 (1962); *The Multifaceted Skyrmion*, edited by G. E. Brown and M. Rho (World Scientific, Singapore, 2010).

[4] S. Mühlbauer, B. Binz, F. Jonietz, C. Pfleiderer, A. Rosch, A. Neubauer, R. Georgii, and P. Böni, Science **323**, 915 (2009).

[5] W. Münzer, A. Neubauer, T. Adams, S. Mühlbauer, C. Franz, F. Jonietz, R. Georgii, P. Böni, B. Pedersen, M. Schmidt, A. Rosch, and C. Pfleiderer, Phys. Rev. B **81**, 041203(R) (2010).

[6] X. Z. Yu, Y. Onose, N. Kanazawa, J. H. Park, J. H. Han, Y. Matsui, N. Nagaosa, and Y. Tokura, Nature (London) **465**, 901 (2010).

[7] X. Z. Yu, N. Kanazawa, Y. Onose, K. Kimoto, W. Z. Zhang, S. Ishiwata, Y. Matsui, and Y. Tokura, Nat. Mater. **10**, 106 (2010).

[8] S. Seki, X. Z. Yu, S. Ishiwata, and Y. Tokura, Science **336**, 198 (2012).

[9] S. Seki, J.-H. Kim, D. S. Inosov, R. Georgii, B. Keimer, S. Ishiwata, and Y. Tokura, Phys. Rev. B **85**, 220406(R) (2012).

[10] S. Seki, S. Ishiwata, and Y. Tokura, Phys. Rev. B **86**, 060403 (2012).

[11] M. C. Langner, S. Roy, S. K. Mishra, J. C. T. Lee, X. W. Shi, M. A. Hossain, Y.-D. Chuang, S. Seki, Y. Tokura, S. D. Kevan, and R. W. Schoenlein, Phys. Rev. Lett. **112**, 167202 (2014).

[12] T. Adams, A. Chacon, M. Wagner, A. Bauer, G. Brandl, B. Pedersen, H. Berger, P. Lemmens, and C. Pfleiderer, Phys. Rev. Lett. **108**, 237204 (2012).

[13] A. A. Omrani, J. S. White, K. Prša, I. Živković, H. Berger, A. Magrez, Y.-H. Liu, J. H. Han, and H. M. Rønnow, Phys. Rev. B **89**, 064406 (2014).

[14] M. R. Eskildsen, E. M. Forgan, and H. Kawano-Furukawa, Rep. Prog. Phys. **74**, 124504 (2011).

[15] S. J. Blundell, Contemp. Phys. **40**, 175 (1999).

[16] J. E. Sonier, J. H. Brewer, and R. F. Kiefl, Rev. Mod. Phys. **72**, 769 (2000).

[17] J.-W. G. Bos, C. V. Colin, and T. T. M. Palstra, Phys. Rev. B **78**, 094416 (2008).

[18] D. B. Williams and C. B. Carter, *Transmission Electron Microscopy* (Springer, New York, 1996), Chap. 28.

[19] F. L. Pratt, Phys. B (Amsterdam) **289**, 710 (2000).

[20] A. Maisuradze, Z. Guguchia, B. Graneli, H. M. Rønnow, H. Berger, and H. Keller, Phys. Rev B **84**, 064433 (2011).

[21] O. Janson, I. Rousochatzakis, A. A. Tsirlin, M. Belesi, A. A. Leonov, U. K. Rößler, J. van den Brink, and H. Rosner, Nat. Commun. **5**, 5376 (2014).

[22] U. K. Rößler, A. N. Bogdanov, and C. Pfleiderer, Nature (London) **442**, 797 (2006).

[23] O. Petrova and O. Tchernyshyov, Phys. Rev. B **84**, 214433 (2011).

[24] M. Mochizuki, X. Z. Yu, S. Seki, N. Kanazawa, W. Koshibae, J. Zang. M. Mostovoy. Y. Tokura, and N. Nagaosa, Nat. Mater. **13**, 241 (2014).

[25] A. N. Bogdanov, U. K. Rössler, and C. Pfleiderer, Phys. B (Amsterdam) **359**, 1162 (2005).

[26] L. Liu, paper presented at MuSR2014, Grindelwald, Switzerland (unpublished) (abstract available from www.psi.ch/musr2014).

[27] R. S. Hayano, Y. J. Uemura, J. Imazato, N. Nishida, T. Yamazaki, and R. Kubo, Phys. Rev. B **20**, 850 (1979).